Water Science & Technology

Water Science & Technology Vol 87 No 3, 748 doi: 10.2166/wst.2023.029

Experiments and simulations of surface cleaning for a gas–liquid two-phase jet

Feng-xia Shi[a], Jian Zhao[b,c,*], Yi Zhou[d] and Huan Zhang[e]

[a] College of Petroleum Engineering, Shandong Institute of Petroleum and Chemical Technology, Dongying 257097, China
[b] Academy of Science and Technology, China University of Petroleum (East China), Dongying 257061, China
[c] School of Petroleum Engineering, China University of Petroleum (East China), Qingdao 266580, China
[d] CNPC Engineering Technology R&D Company Limited, Beijing 102206, China
[e] Committee Organization Department, Xi'an Shiyou University, Xi'an 710065, China
*Corresponding author. E-mail: 000161@sdipct.edu.cn

JZ, 0000-0002-2455-1689

ABSTRACT

In this study, a new cleaning method for the gas-mixed water jet is proposed. The pulsation characteristics of the gas -liquid two-phase jet and the influences of parameters on the cleaning effect were analyzed by performing simulations and experiments. The results showed that the impact pressure fluctuated and was much higher than the inlet pressure. With a continuous increase in the standoff distance, the impact pressure first decreased slowly and then decreased significantly, while the diameter and depth of the crater first increased and then decreased. The optimal standoff distance for a desirable impact effect was 10 mm. With the increase in gas concentration, the impact pressure became higher for gas concentrations of less than 8%, while the impact pressure decreased for the gas concentration of more than 8%. A higher impact pressure along with a fiercer jet pulsation resulted when the flow rate became larger. Accordingly, the diameter and depth of impact crater became enlarged. The impact pressure first increased and then decreased with the increase of nozzle contraction angle. Moreover, the optimal value of such an angle was 140°. This study provides fundamental and practical guidance to further improve the application of gas-mixed water jet cleaning technology.

Key words: cleaning effect, gas-mixed water jet cleaning, impact force, jet parameters optimization, pulsation characteristics

HIGHLIGHTS

- A method for surface cleaning of a gas-mixed water jet was proposed.
- The impact pressure of the gas–liquid two-phase jet was greater than that of the pure water jet.
- The pulsation characteristics of the gas–liquid two-phase jet was revealed.
- An optimal standoff distance existed for the gas–liquid two-phase jet cleaning.
- An optimal gas concentration is obtained for the desired impact effect.

GRAPHICAL ABSTRACT

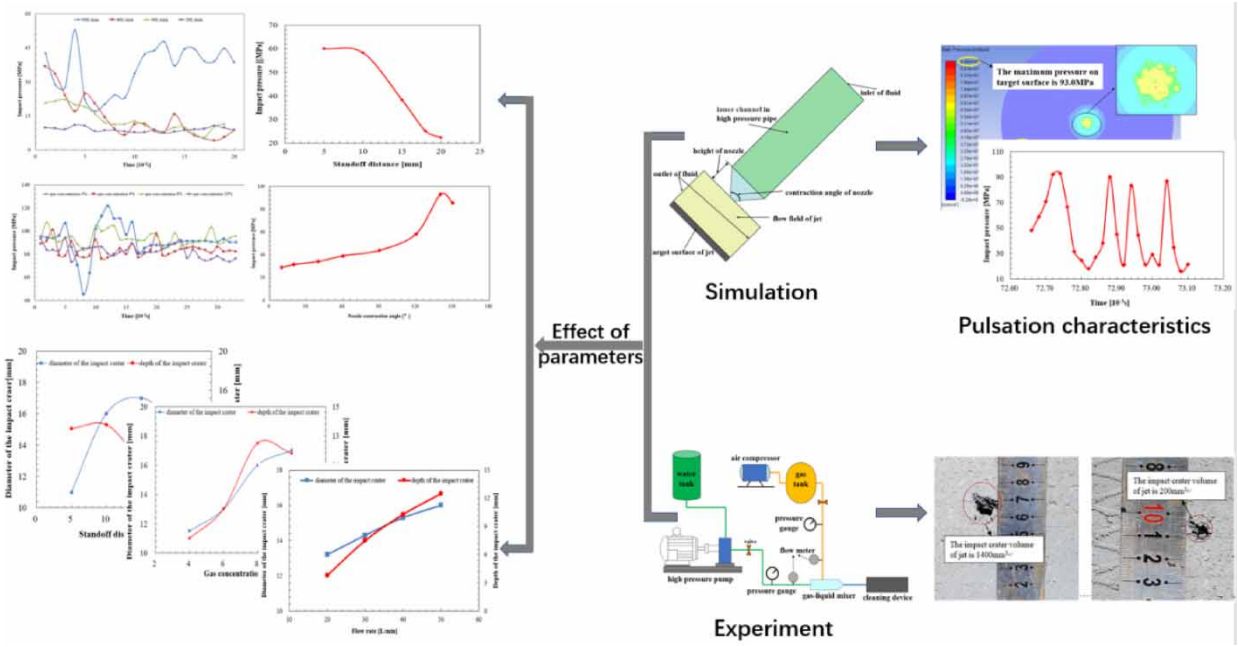

1. INTRODUCTION

Tubing is widely used in oil and gas production operations and plays an extremely important role in the petroleum industry as a conduit conveying oil and gas from underground to the surface. Tubing accounts for more than 10% of the steel used in the petroleum industry, whereas the expense of tubing accounts for a large proportion of the development cost of petroleum (Shen 2018). Due to high temperature and high pressure in the downhole, dirt and rust are easily formed on the surface of the tubing, resulting in the decline of the oil well's productivity, the sticking of well string, frequent disconnections, and the shortening of pump's inspection cycle. Consequently, the cost of oil and gas production increases, resulting in a decline in the economic benefits of the oil field. Practically, the production costs of oil and gas can be greatly reduced by applying tubing repair technology. As the most basic aspect of tubing repair technology, the efficiency of the tube cleaning technology directly affects the quality of the repaired tubing (Feng *et al.* 2010). Therefore, in-depth studies focusing on efficient tubing cleaning technology are of particular interest to researchers and engineers.

In recent years, the high-pressure water jet cleaning technology has been widely studied and applied due to its advantages of simple process, environment-friendliness, and high cleaning efficiency (Thomas 1995; Lu & Chen 2004; Song *et al.* 2014; Zhao *et al.* 2017a, 2017b; Singh *et al.* 2021). The mechanism of such a cleaning has been analyzed and the cleaning device has been introduced in a previous work (Xue *et al.* 2008). Cleaning tests using high-pressure water jet were carried out on tube coatings and workpieces with different hardness values (Guo *et al.* 2014), and it was found that, when a crack existed at the surface of the coating, the cleaning speed increased linearly, while the increase of cleaning speed resulted in an increase in the surface roughness of the tube. For the high-pressure water jet technology, experimental studies have been conducted to evaluate the effectiveness of the tools for the removal of surface attachments. Under the pressure of 60 MPa, with the nozzle diameter of 1.4 mm and the dwell time of 60 s, the surface attachments could be cleaned up efficiently (Huang *et al.* 2014). Based upon pre-mixed abrasive water jet, the internal flow field of the mixing chamber of the nozzle was numerically simulated, while reasonable structural parameters were obtained to improve the mixing homogeneity of the water jet (Liu *et al.* 2014). The rust and dirt covering the body of a truck were removed using abrasive water jet technology (Zuo & Liu 2014). The movement of abrasive particles in the water jet and the wear of abrasive particles on the nozzle were simulated, the results of which were used to optimize the structure of the nozzle (Deng *et al.* 2021; Du *et al.* 2021). The influence of inlet disturbance on the performance of the self-excited oscillation cavitation nozzle was evaluated by analyzing the peak value of axial pressure fluctuations and the jet's erosion intensity (Li *et al.* 2016). The flow field of a new type of Helmholtz nozzle was

numerically simulated using computational fluid dynamics (CFD) and the factors dominating the cavitation jet effect, including nozzle cavity height, cavity width, expansion tube angle, and pump rated pressure were analyzed (Qi *et al.* 2020). By taking the tandem double-chamber self-excited oscillating pulse nozzle as the research object, the influence of the nozzle's structural parameters on the internal flow field of the cavitation jet was simulated (Sun *et al.* 2019). Due to their distinct advantages, various water jet technologies have been applied in many fields. However, the extremely high pressure (more than 150 Mpa) of the pure water jet technology poses challenges to equipment safety and also increases the pumping cost. The impact and grinding effects of an abrasive water jet are much better than those of a pure water jet. However, in the case of the former, various problems such as serious wear of cleaning equipment and nozzle, difficulty in recycling, and utilization of abrasives are frequently encountered. The strong impact force can be generated by the cavitation effect in the cavitation jet technology, while the cavitation effect is subject to a nozzle's structure. A certain amount of jet energy will be consumed due to the occurrence of spontaneous cavitation, which consequently reduces the cleaning efficiency. Comparatively, the gas–liquid two-phase jet is a cleaning method having a higher efficiency.

The gas–liquid two-phase jet technology was proposed by Eddingfield and Albrecht from the University of Illinois in the United States (Eddingfield *et al.* 1979). The mixed gas reduced the frictional resistance between the water jet and the surrounding environment, which improved the effective target distance. Later, the study on the impact of the gas–liquid two-phase jet on concrete specimens showed that, compared with the pure water jet, the peak pressure of gas–liquid two-phase jet on the surface of specimens remained unchanged and its erosion performance was greatly increased (Momber 2000). An optimal gas concentration maximized the erosion, while the crack area on the specimen's surface expanded obviously. Based on this technology, the former Soviet Academy of Sciences proposed the gas–liquid pulse jet rock-breaking method by changing the structural parameters and jet medium of the pulse water jet device and obtained a 27% higher effect than the ordinary pulse jet (Wang & Zhou 1988). Teruo & Hiroshi (1977) systematically studied the fluid characteristics of gas–liquid two-phase jet under submerged conditions and applied it to high-pressure rotary jet grouting technology. Based upon CFD, the morphological characteristics of the gas–liquid two-phase jet were numerically simulated after injecting compressed air into the water jet, and the experiments were carried out to verify the simulation results (Annoni *et al.* 2014). The mixing of a certain amount of compressed air is not only beneficial in enhancing the stability of jet flow and maintaining the consistency of a jet's structure, but also in improving the cutting quality and enhancing the cutting capability of the jet. The ability of a gas to protect the jet was studied using simulations and experiments, which showed that, compared to the pure water jet, the protective gas can reduce the jet's frictional resistance, reduce the energy loss, and greatly improve the effective target distance of the jet under submerged conditions (Li 2008). The gas–liquid two-phase jet was applied to the hydraulic fracture-cutting technology of coal and the device for gas–liquid two-phase jet fracture-breaking was designed and developed (Lin *et al.* 2018). Compared with the pure water jet, the pressure threshold of the gas–liquid two-phase jet coal-cracking was reduced, whereas the depth and the diameter of the crushing crater were twice those of the pure water jet.

Previous studies have mainly focused on the applications of a gas–liquid two-phase jet in the fields of rotary jet grouting and rock-breaking, whereas less focus has been dedicated to the field of cleaning. In this study, the gas–liquid two-phase jet technology has been used to obtain an optimum cleaning efficiency. Based on the VOF (volume of fluid) model, the flow field characteristics of gas–liquid two-phase jet and the influence of the variation of jet parameters on the cleaning effect were analyzed using numerical simulations. The results were verified using experiments. The simulation results provide theoretical guidance for the application of two-phase jet cleaning technology.

2. NUMERICAL MODEL

2.1. Governing equations

Based upon a fixed Euler grid, the VOF model can achieve surface-tracking in the simulations. The phase interface of each cell can be tracked by introducing a variable called phase volume fraction. The VOF model has the advantages of easy implementation, small requirements for computational power, and high precision, which is due to the reason that it tracks the fluid volume in the grid rather than the motion of the fluid particle. Therefore, the VOF model was employed to simulate the flow field characteristics of the gas–liquid two-phase jet and the influence of jet parameters.

The governing equations of the VOF model are presented as follows (Li & Shao 2018):

(1) Continuity equation is given by Equation (1):

$$\frac{\partial \rho}{\partial t} + \nabla \cdot (\rho \boldsymbol{u}) = 0 \tag{1}$$

where $\boldsymbol{u}$ is the vector of velocity, ρ is the density of fluid, and $\bigtriangledown$ is the Hamiltonian.

(2) Momentum equation is given by Equation (2):

$$\frac{\partial (\rho \boldsymbol{u})}{\partial t} + \nabla \cdot (\rho \boldsymbol{u}\boldsymbol{u}) = -\nabla p + \nabla \cdot [\mu(\nabla \boldsymbol{u} + \nabla \boldsymbol{u}^T)] + \rho g + \boldsymbol{F} \tag{2}$$

where $\boldsymbol{u}$ is the vector of velocity, ρ is the density of the fluid, μ is the viscosity of the fluid, $\mathbf{g}$ is the gravitational volume force, and $\boldsymbol{F}$ is the external volume force.

(3) Equation of volume fraction is given by Equation (3):

For phase q:

$$\frac{\partial \alpha_q}{\partial t} + u \cdot \nabla \alpha_q = \frac{s_{\alpha_q}}{\rho_q} \tag{3}$$

The volume fraction of the main phase is calculated based on the constraints given in Equation (4):

$$\sum_{q=1}^{n} \alpha_q = 1 \tag{4}$$

where α_q is the volume fraction of phase q and s_{α_q} is the quality source item.

(4) Turbulence mode

Standard k–ε model is utilized to calculate the turbulence of the fluid (Zhao *et al.* 2018) and is given by Equations (5) and (6):

$$\frac{\partial (\rho k)}{\partial t} + \frac{\partial (\rho k u_i)}{\partial x_i} = \frac{\partial}{\partial x_j}\left[\left(\mu + \frac{\mu_t}{\sigma_k}\right)\frac{\partial k}{\partial x_j}\right] + G_k - \rho\varepsilon + S_k \tag{5}$$

$$\frac{\partial (\rho \varepsilon)}{\partial t} + \frac{\partial (\rho \varepsilon u_i)}{\partial x_i} = \frac{\partial}{\partial x_j}\left[\left(\mu + \frac{\mu_t}{\sigma_\varepsilon}\right)\frac{\partial \varepsilon}{\partial x_j}\right] + \frac{C_{1\varepsilon}\varepsilon}{k} G_k - C_{2\varepsilon}\rho\frac{\varepsilon^2}{k} + S_\varepsilon \tag{6}$$

where x is the spatial coordinate in tensor form, k is the turbulent kinetic energy, G_k is the generation term of turbulent kinetic energy caused by the velocity gradient of laminar, σ_k and σ_ε are the turbulent Prandtl numbers of k equation and ε equation, respectively, ε is the turbulent dissipation rate, $\mu_t = C_\mu \rho k^2/\varepsilon$ is the turbulent viscosity, $C_{1\varepsilon}$, $C_{2\varepsilon}$ are the empirical coefficients, and S_k, S_ε are the source terms. $C_{1\varepsilon} = 1.44$, $C_{2\varepsilon} = 1.92$, $C_\mu = 0.09$, $\sigma_k = 1.00$, and $\sigma_\varepsilon = 1.30$ (Shamshirband *et al.* 2015; Zhao *et al.* 2017a, 2017b).

2.2. Physical model and meshing

The physical model of gas–liquid two-phase jet is shown in Figure 1(a). The nozzle diameter d is 2 mm, whereas the nozzle height h is 4 mm. Moreover, the flow channel length in high-pressure pipe L is 150 mm. The model was divided using unstructured hexahedral mesh, and the number of nodes was 210,132. Furthermore, the size of the mesh was 1 mm and the local mesh refinement technique was applied, as shown in Figure 1(b).

2.3. Assumption and boundary condition

The ANSYS Fluent 18.2 was used to simulate the flow field characteristics and cleaning effects of the gas–liquid two-phase jet. Various assumptions were made for the analysis, and they are given as follows: (1) the mass transfer and heat transfer between the two phases were ignored; (2) No heat exchange occurred between the fluid and the external medium, and

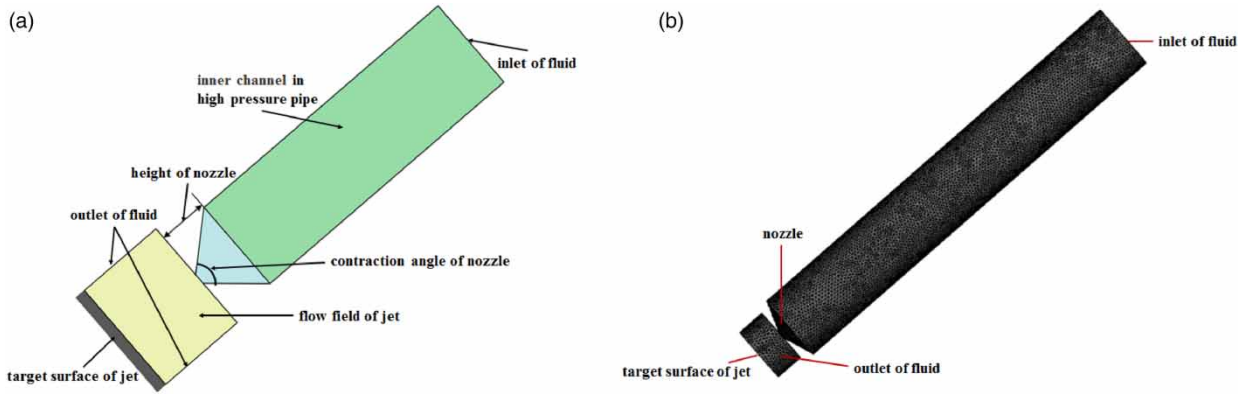

Figure 1 | (a) Physical model of the gas–liquid two-phase jet and (b) its meshing model.

(3) the temperature remained constant. The boundary conditions were set as follows: velocity-inlet (to investigate the targeted velocity field of the gas–liquid two-phase flow in detail), and pressure-outlet. Additionally, the pressure at the outlet was zero.

3. EXPERIMENT

3.1. Experimental setup

The ground tests of gas–liquid two-phase jet cleaning were carried out to verify the numerical results. The experimental devices mainly included a water tank, high-pressure pump, air compressor, air tank, gas–liquid mixture, and cleaning nozzle (see Figure 2). Before entering the cleaning nozzle, the air was pre-mixed with the fluid. The air compressed by the air compressor was transported into the gas tank and then it was mixed with the high-pressure water that was pressurized by the high-pressure pump in the gas–liquid mixer. Both the air and fluid flow rates were measured using flowmeters. The gas–liquid two-phase (mixture) jet was generated (ejection) by the nozzle to clean the targeted surface.

3.2. Jet parameters

The variation of impact effect with certain jet parameters was investigated, such as the standoff distance (the distance between the nozzle outlet and the target surface), which varies within the range of 5–20 mm. The gas concentration is defined as the gas volume fraction in the gas–liquid two-phase jet (referred to as the gas volume fraction of the inlet), and varied within the range of 4–10%. The flow rate of the liquid laid within the range of 20–50 L/min. The nozzle contraction angle (tapered angle of the converging nozzle) laid within the range of 10–140° (see Table 1).

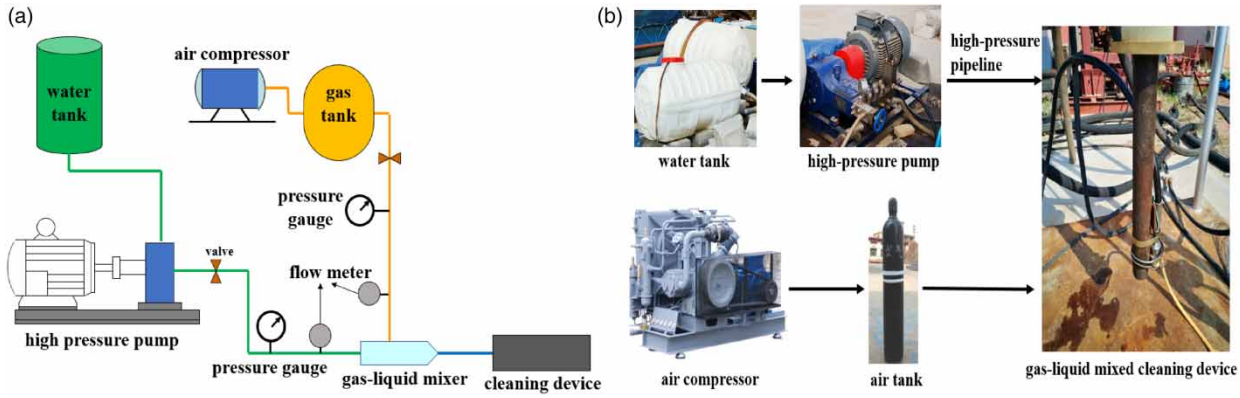

Figure 2 | (a) Schematic of the gas–liquid two-phase jet cleaning test and (b) photographs of various devices used in the experimental setup.

Table 1 | Various parameters for the simulation and experiments

	Standoff distance (mm)	Gas concentration (%)	Flow rate (L/min)	Nozzle contraction angle (°)
Simulation	5–20	4–10	20–50	10–150
Experiments	5–20	4–10	20–50	–

4. RESULTS AND ANALYSIS

4.1. Flow field characteristics

4.1.1. Pulsation characteristics

Simulations were performed with the inlet gas concentration of 8% in the two-phase jet, the flow rate of 50 L/min, the nozzle contraction angle of 140°, and the standoff distance of 10 mm. The liquid phase was divided into many segments by the gas phase, showing the pulsation characteristics of the jet (see Figure 3(a)). Figure 3(b) shows that the velocity of the fluid changed slightly in the pipeline, whereas it increased rapidly at the outlet of the nozzle. The variation of impact pressure (impact pressure is defined as the maximum pressure acting on the targeted surface) by gas–liquid two-phase jet with time is shown in Figure 3(c). The impact pressure acting on the targeted surface fluctuated within the range of 16–93 MPa, showing an irregular pulsation characteristic. This instantaneous higher pressure (much higher than the inlet pressure, i.e., 49.3 MPa) with tremendous energy could efficiently break the dirt and rust. The gas phase existed in the form of irregular micro-bubbles within the gas–liquid two-phase jet, and accordingly, the liquid phase was divided into discontinuous liquid columns by

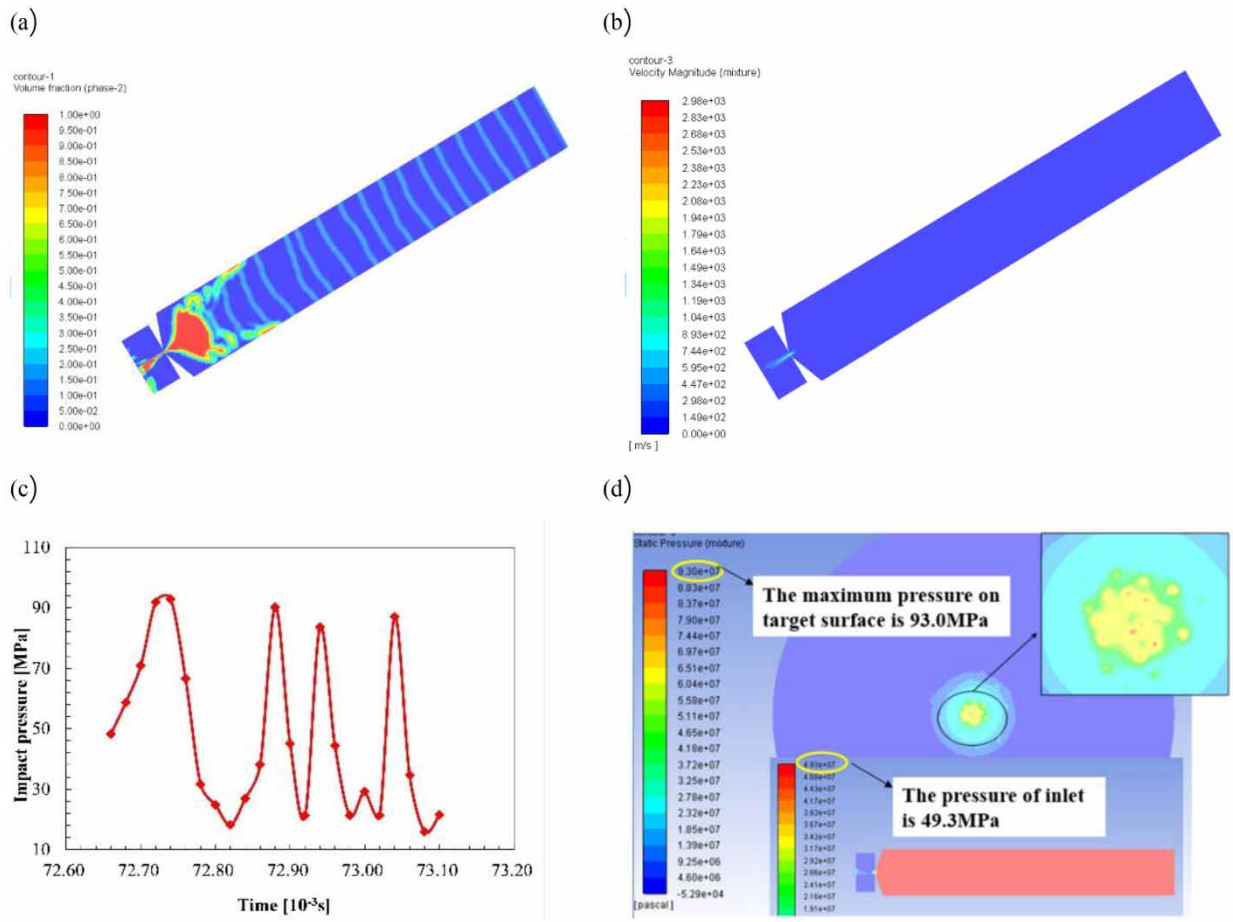

Figure 3 | (a) Volume fraction of the gas phase in the gas–liquid two-phase jet, (b) velocity contour, (c) variation of impact pressure by the gas–liquid two-phase jet with time, and (d) pressure nephogram obtained from the simulation results.

the gas phase. Therefore, a strong impact effect can be produced when the liquid column impacts the targeted surface at an extremely high speed. The discontinuity of the liquid columns caused a strong shock wave, resulting in a sudden increase in pressure that acted on the targeted surface (Shen 1998; Lin *et al.* 2018). Therefore, with this pulsation effect, the cleaning effect can physically be improved greatly.

4.1.2. Impact pressure

For the gas concentration, flow rate, nozzle contraction angle and standoff distance of 8%, 50 L/min, 140°, and 10 mm, respectively, the simulated pressure nephogram of the gas–liquid two-phase jet is shown in Figure 3(d). The impact pressure (93.0 MPa) acting on the targeted surface was much higher than the inlet pressure (49.3 MPa). This can be ascribed to the fact that a micro jet with a high velocity is formed and a water hammering effect is generated when the intermittently distributed liquid columns impact on the targeted surface. As a result, the extremely instantaneous pressure becomes much greater than the stagnation pressure, which greatly improves the impact effect of the gas–liquid two-phase jet (Wang 2010).

The cement blocks were utilized as the impact targets to compare the impact effects between the gas–liquid two-phase jet and the pure water jet. The impact effects of gas–liquid two-phase jet and pure water jet are compared (see Figure 4). When the flow rate, standoff distance, gas concentration and nozzle contraction angle had values of 50 L/min, 10 mm, 8%, and 140°, respectively, the impact crater volume of the gas–liquid two-phase jet (1,400 mm^3) was about seven times that of the pure water jet (200 mm^3) under the same conditions. The reasons accounting for the higher (much greater than that of the pure water jet) impact force during the gas–liquid two-phase jet have been discussed above. Moreover, the crater area of the gas–liquid two-phase jet was larger than that of the pure water jet, again indicating that the cleaning efficiency of the gas–liquid two-phase jet was higher than that of the pure water jet.

4.2. Effect of jet parameters

To identify the jet parameters of a gas–liquid two-phase jet, sensitivity analysis based on numerical simulations combined with laboratory experiments was implemented. Various factors such as the standoff distance, gas concentration, flow rate, and nozzle contraction angle were used in the analysis.

4.2.1. Standoff distance

When the nozzle contraction angle, flow rate and gas concentration had values of 140°, 50 L/min, and 8%, respectively, the influence of the standoff distance on the impact pressure acting on the targeted surface was simulated, and the corresponding results are shown in Figure 5(a). With an increase in the standoff distance, the impact pressure remained almost unchanged, and decreased rapidly only when the standoff distance exceeded the value of 10 mm. When the standoff distance was less than 10 mm, the targeted surface was located inside the jet potential core, where the jet velocity was extremely high.

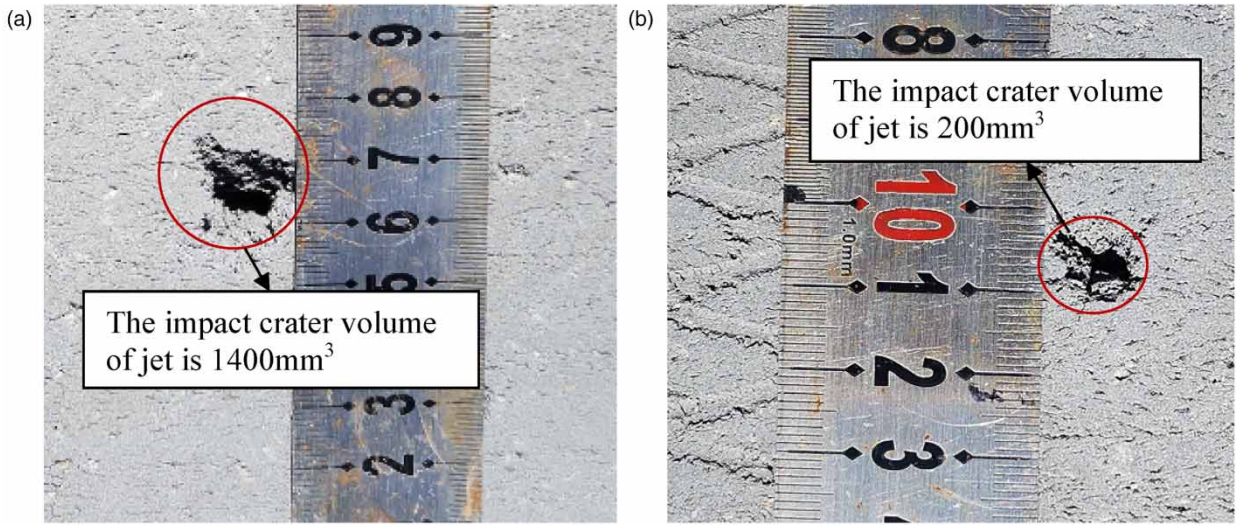

Figure 4 | Impact effect comparison of the (a) gas–liquid two-phase jet and (b) pure water jet.

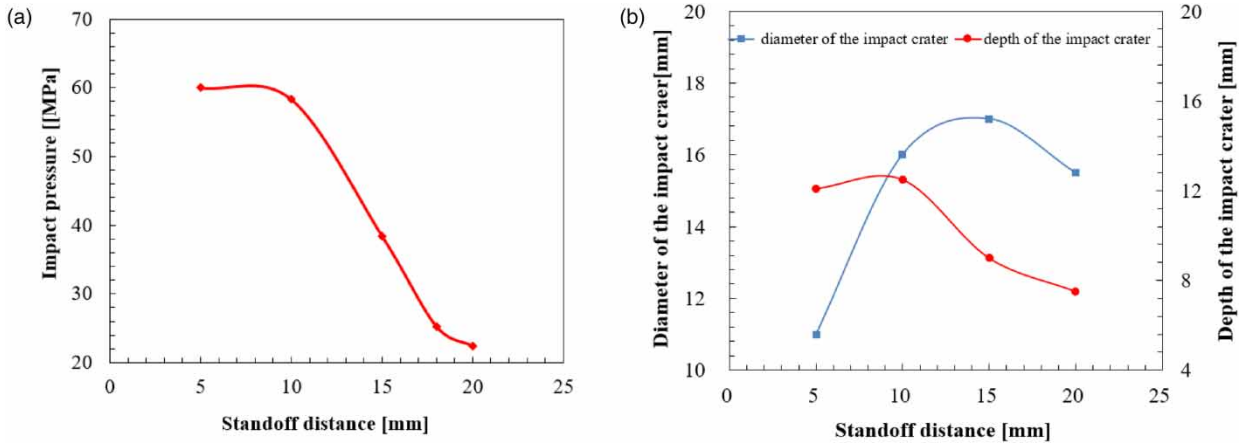

Figure 5 | Results with different standoff distances: (a) simulated impact pressure and (b) experimental impact crater size versus the standoff distances.

Under this condition, most of the kinetic energy of the jet was converted into stagnation pressure energy on the targeted surface, resulting in a greater impact force (Ni 2012). As the standoff distance continued to increase, the targeted surface went outside the potential core, which caused a significant reduction in the jet velocity. For this distance, part of the jet's kinetic energy was consumed by the air resistance, while the jet's energy was dispersed. As a result, the stagnation pressure energy on the targeted surface decreased. However, the smaller the standoff distance, the smaller the effective action area of the jet. Practically, by balancing both the aspects of the impact pressure and the effective action area, the optimal standoff distance was determined to be 10 mm (five times that of the nozzle diameter).

The experimental results are shown in Figure 5(b). For the flow rate, gas concentration and impact time of 50 L/min, 8%, and 60 s, respectively, the dependence of the diameter and depth of the impact crater on the standoff distance are depicted in Figure 5(b). With the increase in the standoff distance, the depth of the impact crater slightly increased followed by a decrease, while the diameter of the impact crater first increased and then decreased. When the standoff distance was smaller than 10 mm, the targeted surface was located inside the jet's potential core area. The jet velocity arriving at the targeted surface was almost uniform. Therefore, the crater diameter slightly increased. As the standoff distance exceeded the value of 10 mm, the targeted surface went outside the core area, so that the impact velocity and pressure began to decrease quickly, thus decreasing the crater diameter. The crater diameter reached its maximum value when the standoff distance was 15 mm. When the standoff distance was smaller than 15 mm, the gas–liquid two-phase jet energy was slightly dispersed. Meanwhile, the overall energy was concentrated, which led to an increase in the crater diameter. However, as the standoff distance became larger than 20 mm, the gas–liquid two-phase jet energy dispersed significantly. Therefore, parts of the jet energy were not strong enough to break the cement block, which led to a decrease in the crater diameter. To sum up, combining the impact pressure with the carter depth and diameter, the optimum standoff distance was chosen to be 10 mm (five times that of the nozzle diameter).

4.2.2. Gas concentration

When the nozzle contraction angle, flow rate and standoff distance had values of 140°, 50 L/min, and 10 mm, respectively, the impact pressure was simulated as a function of time for different gas concentrations, and the corresponding results are presented in Figure 6(a). When the gas concentration was 4%, the fluctuation of impact pressure was more pronounced initially, and then, weakened significantly over a long period, indicating a discontinuous pulsation. On the other hand, the pulsation was continuous for the gas concentration values of 6–10%. Therefore, the impact effect of the gas–liquid two-phase jet was better for the gas concentration of more than 4%. When the gas concentration laid within the range of 6–10%, the maximum impact pressure first increased, and then, decreased with the increase in gas concentration. With the increase of gas concentration, the number of bubbles in the jet gradually increased, leading the gas bubbles to be more easily deformed and collapsed, due to which, the fluctuation occurred at full time, as shown in Figure 6(a). The bursting of bubbles enhanced the jet energy (Xiang *et al.* 2006; Shi *et al.* 2021), which resulted in the increase of jet pressure

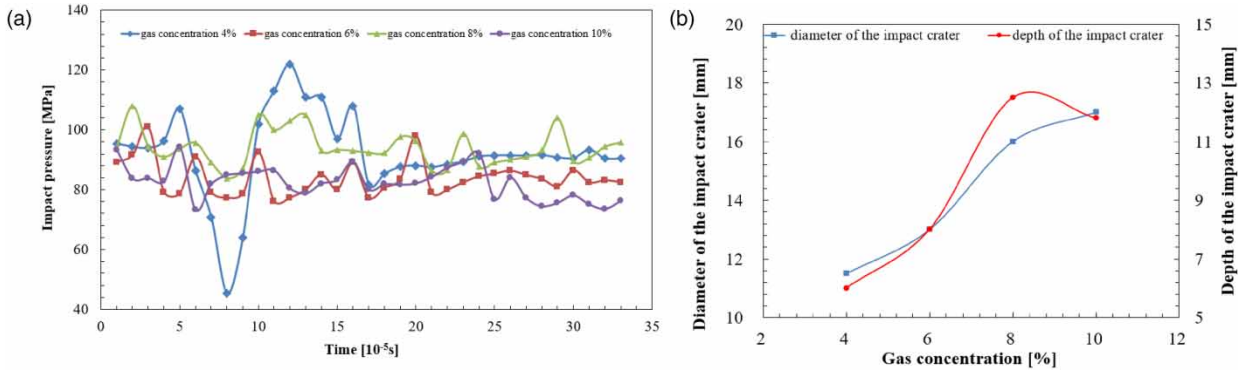

Figure 6 | (a) Simulated impact pressure and (b) experimental diameter and depth of the impact crater under various gas concentrations.

acting on the targeted surface. However, when the gas concentration exceeded the value of 8%, the liquid phase energy was dispersed greatly by the gas phase, resulting in the decrease of impact pressure acting on the targeted surface. Therefore, under the simulation conditions, a better impact effect of the gas–liquid two-phase jet can be achieved for the gas concentration of around 8%.

For the flow rate, standoff distance and impact time of 50 L/min, 10 mm, and 60 s, respectively, the experimental diameter and the depth of the impact crater under different gas concentrations are depicted in Figure 6(b). With the increase in gas concentration, the diameter of the impact crater increased, while the depth of the impact crater first increased, and then, decreased. With the increase in gas concentration, the liquid phase was more dispersed by the gas phase, resulting in a gradual increase of the jet's action area on the targeted surface and the diameter of the impact crater. When the gas concentration was less than 8%, the jet had a strong clustering property. With the increase in gas concentration, the impact force generated by bubble bursting enhanced the jet's energy, resulting in an increase in the depth of the impact crater. As the gas concentration continued to increase, the liquid energy was seriously dispersed by the gas phase, which decreased the jet impact force and the impact crater depth.

4.2.3. Flow rate

For the nozzle contraction angle, gas concentration, and standoff distance of 140°, 8%, and 10 mm, respectively, the influence of the flow rate on the impact pressure acting on the targeted surface is shown in Figure 7(a). When the flow rate was 20 L/min, the impact pressure changed insignificantly with time. With the increase in the flow rate, the impact pressure gradually increased, and the pulsation feature began to appear. At the flow rate of 50 L/min, the impact pressure and the pulsation effect became the highest and the most obvious, respectively. The larger the flow rate, the higher the jet energy, and therefore, the more obvious the pulsation characteristics and the greater the impact force on the targeted surface. Therefore, it

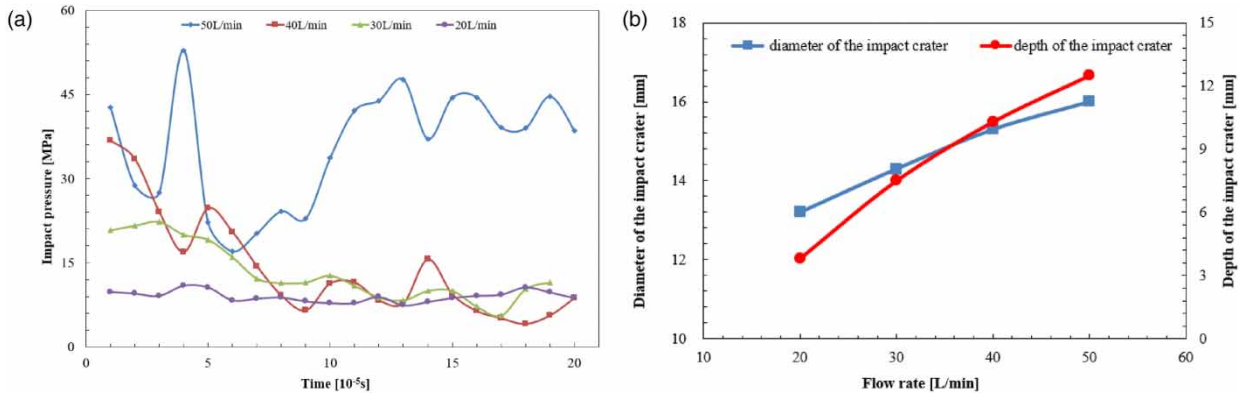

Figure 7 | (a) Simulated impact pressure and (b) experimental diameter and depth of the impact crater under different flow rates.

can be inferred that the flow rate of the jet should be increased as much as possible to improve the cleaning efficiency provided the field equipment capacity allows it.

For the gas concentration, standoff distance, and impact time of 8%, 10 mm, and 60 s, respectively, the experimental diameter and the depth of the impact crater under various flow rates are depicted in Figure 7(b). The results showed that, with the increase in the flow rate, the diameter and the depth of the impact crater gradually increased. This is because the larger flow rate was accompanied with a higher jet energy, resulting in a larger impact force. Therefore, if the capacity of field equipment allows, the flow rate should be as high as possible to maximize the cleaning efficiency.

4.2.4. Nozzle contraction angle

Due to the complexity of experiments with different nozzle contraction angles, the influence of nozzle contraction angle on gas–liquid two-phase jet was examined using numerical simulation.

For the flow rate, gas concentration, and standoff distance of 50 L/min, 8%, and 10 mm, the simulated impact pressure (acting on the targeted surface) with nozzle contraction angles is shown in Figure 8. With the increase of nozzle contraction angle, the impact pressure on the targeted surface first increased, and then, decreased, reaching the maximum at the angle of 140°. With the increase of nozzle contraction angle, the larger velocity-change of the gas–liquid two-phase jet flowing through the nozzle was observed, which led to a significant increase in the pressure. This way, the probability of bubble aggregation and collapse increased, and the jet's impact force was greatly enhanced by the cavitation effect. For a further increase in the nozzle contraction angle, the jet's energy loss caused by the structure of the nozzle became dominant because the local resistance coefficient of the nozzle increased rapidly, resulting in a decrease in the impact pressure acting on the wall despite the fact that the jet's energy increased.

4.2.5. Target performance

The cleaning effect will also be affected by the physical properties/conditions of the cleaning target (Figure 9). When primary pores or cracks exist in the target, the area of the impact crater is larger than those targets without the existence of such pores or cracks. Therefore, the cleaning speed will be faster if the pores or cracks exist in the coating or rust/scale layer.

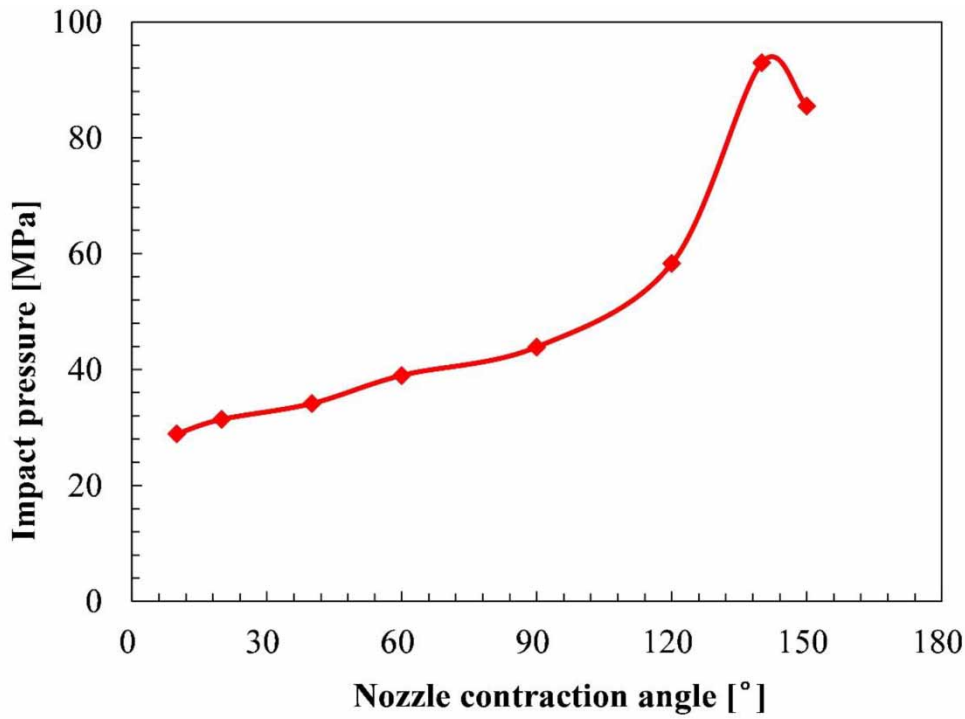

Figure 8 | Variations in the impact pressure with nozzle contraction angle.

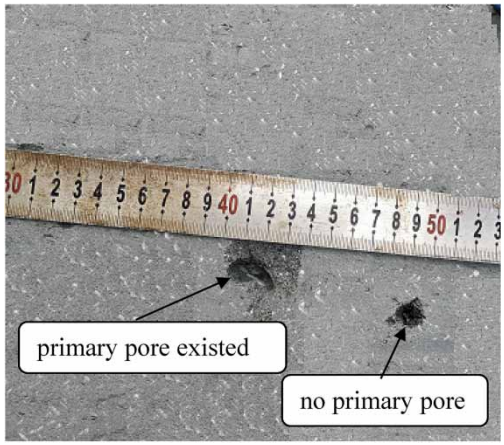

Figure 9 | Influence of target performance on the jet effect.

5. CONCLUSIONS

In this study, a new cleaning method of gas-mixed water jet was proposed. Experimental and numerical methods were used to evaluate the cleaning effect of the gas-mixed water jet by analyzing different parameters. Major findings can be summarized as follows:

- The impact pressure of the gas–liquid two-phase jet acting on the targeted surface fluctuated with time, and exhibited obvious pulsation characteristics. The impact pressure of the gas–liquid two-phase jet was much higher than the inlet pressure.
- With the increase of standoff distance, the impact pressure acting on the targeted surface remained almost unchanged. However, when the standoff distance exceeded the value of 10 mm, the pressure decreased rapidly. The optimal standoff distance was determined to be 10 mm. The impact pressure firstly increased and then decreased with the increase of gas concentration for the concentration range of 6–10%. The desirable impact effect can be obtained when the gas concentration was about 8%. The larger flow rate yielded a greater impact pressure together with more obvious pulsation characteristics. Moreover, the diameter and the depth of the impact crater increased. With the increase in nozzle contraction angle, the impact pressure acting on the targeted surface first increased and then decreased, while the optimal contraction angle was numerically determined to be 140°.
- The jet cleaning effect is better if primary pores or cracks exist in the targeted surface. Therefore, the cleaning speed can be increased when pores or cracks exist in the coating or rust/scale layer.

ACKNOWLEDGEMENTS

This work was financially supported by the National Natural Science Foundation of China (No. 52204022), the Natural Science Foundation of Shandong Province (No. ZR2022ME152), the National Key Research and Development Program of China (No. 2021YFE0111400), the Fundamental Research Funds for the Central Universities (No. 19CX02063A), and the Science and Technology Plan of Dongying City (No. 2021ZD49).

DATA AVAILABILITY STATEMENT

All relevant data are included in the paper or its Supplementary Information.

CONFLICT OF INTEREST

The authors declare there is no conflict.

REFERENCES

Annoni, M., Arleo, F. & Malmassari, C. 2014 CFD aided design and experimental validation of an innovative Air Assisted Pure Water Jet cutting system. *J. MATLS Proc. Technol.* **214** (8), 1647–1657. https://doi.org/ 10.1016/j.jmatprotec.2014.01.020.

Deng, J. S., Yuan, Y. F., Li, D. R., Cheng, H., Dai, C., Shen, J., Xie, F. & Wang, J. S. 2021 Optimization of abrasive water jet nozzle based on numerical simulation. *J. Phys. Conf. Series* **587**, 12–14. https://doi.org/10.1088/1742-6596/1985/1/012014.

Du, M. M., Wang, H. J., Dong, H. Y., Guo, Y. J. & Ke, Y. L. 2021 Numerical research on multi-particle movements and nozzle wear involved in abrasive waterjet machining. *Int. J. Adv. MFG Technol.* **117** (9/10), 2845–2858. https://doi.org/10.21203/rs.3.rs-186455/v1.

Eddingfield, D. L., Albrecht, Heymann, J. F., Selberg, P. B. & Barber, P. J. 1979 Effect of an air-Injected shroud on the breakup length of a high- velocity waterjet. *ASTM Spec. Tech. Publ.* **664**, 461–472. https:// doi.org/10.1520/STP35812S.

Feng, D., Huang, C. B., Li, S. Y., Li, Y. & Cao, Z. Q. 2010 Application and research of tubing cleaning technology. *Fault-block Oil Gas F.* **17** (1), 102–104. (in Chinese).

Guo, Q., Li, F. Y., Li, S. & Nie, Y. Y. 2014 Research on decontamination effect and damage of high- pressure water jet cleaning to matrix. *China Mech. Eng.* **25** (6), 817–820. Available from: http://www.cmemo.org.cn/CN/Y2014/V25/I6/817.

Huang, Y. Y., Fu, Y. B., Meng, Z. L., Shi, Y. F., Wei, S. S., Yang, F. J. & Zhu, Y. Y. 2014 Research on cleaning cutting tools with high pressure water jet. *Shanghai Nonf. Metals* **35** (1), 20–23. (in Chinese).

Li, J. Y. 2008 *Study on Characteristics of Gas Shrouded Water Jet and Rock-Erosion Experiments*. China University of Petroleum Press, Dongying, China.

Li, C. Q. & Shao, C. L. 2018 Visualization experiment and numerical simulation of gas-liquid two phase flow in a low specific speed centrifugal pump. *J. Cent. South Univ.* **49** (11), 2877–2885. https://doi.org/10.11817/j.issn.1672-7207.2018.11.030.

Li, D., Kang, Y. & Ding, X. 2016 Effects of area discontinuity at nozzle inlet on the characteristics of self-resonating cavitating water jet. *Chin. J. Mech. Eng.* **29** (4), 813–824. https://doi.org/10.1016/j.expthermflusci.2016.07.013.

Lin, B. Q., Wang, R. & Qiao, S. H. 2018 Characteristics and mechanism of multistage fluctuation of coal-breaking caused by high-pressure gas-liquid two-phase jet. *J. China Coal Soc.* **43** (1), 124–130. https://doi.org/10.13225/j.cnki.jccs.2017.4305.

Liu, G. Y., Chen, X. N., Zhu, D. M., Zhang, S. J. & Chen, J. D. 2014 Internal mixing chamber flow field of a premixed abrasive water jet descaling nozzle. *J. Univ. Sci. Technol. Beijing* **36** (6), 830–837. https://doi.org/10.13374/j.issn1001-053x.2014.06.018.

Lu, J. B. & Chen, J. 2004 Selection for cleaning parameters based on distribution of high-pressure waterjet. *China Saf. Sci. J.* **14** (12), 67–70. · https://doi.org/10.16265/j.cnki.issn1003-3033.2004.12.014.

Momber, A. W. 2000 Concrete failure due to air-water jet impingement. *J. MATLS Sci.* **35** (11), 2785–2789. https:// doi.org/ 10.2118/4247-PA.

Ni, L. Y. 2012 *Engineering Fluid Mechanics*. China University of Petroleum Press, Dongying, China.

Qi, M., Wang, L. F., Chen, Q. G., Zhao, J. L., Ju, Y. H. & Fu, Q. Q. 2020 Numerical simulation of cavitating jet in dual chamber self-oscillation pulse nozzle. *J. Dnge. Irrigation Mach. Eng.* **38** (5), 457–461. https://doi.org/10.3969/j.issn.1674-8530.19.0034.

Shamshirband, S., Malvandi, A., Karimipour, A., Goodarzi, M., Afrand, M., Petković, D., Dahari, M. & Mahmoodian, N. 2015 Performance investigation of micro- and nano-sized particle erosion in a 90° elbow using an ANFIS model. *Powder Technol.* **284**, 336–343. https://doi.org/10.1016/j.powtec.2015.06.073.

Shen, Z. H. 1998 *Water Jet Theory and Technology*. University of Petroleum Press, Dongying, China.

Shen, G. H. 2018 Application of tubing restore and recycle technology. *Tianjin Sci. Technol.* **45** (4), 87–88. https://doi.org/10.14099/j.cnki.tjkj.2018.04.027.

Shi, F. X., Zhao, J., Sun, X. G. & Yin, H. L. 2021 Numerical simulation of surface cleaning flow field for gas-liquid two-phase jet. *J. Cent. South Univ.* **52** (3), 960–970. https://doi.org/10.11817/j.issn.1672-7207.2021.03.027.

Singh, N. P., Srinivasu, D. S. & Babu, N. R. 2021 Modelling of abrasive waterjet kerf in a double-layered structure. *J. Manuf. Process* **69**, 514–531. https://doi.org/10.1016/j.jmapro.2021. 07.053.

Song, J. H., Liu, C. L., Xu, S. T., Wu, G. & Wang, C. D. 2014 Cleaning technique with high pressure water jet and its application in removing scale in piping. *Process Equip. Pip.* **51** (5), 79–82. (in Chinese).

Sun, P. F., Zhou, Z. Q., Chen, Y., Jiang, Z., Luo, G. S. & Wang, B. 2019 Parametric study on self-excited vibration cavitation jet nozzles based on the CFD method. *Fluid Mach.* **47** (10), 1–7. https://doi.org/10.3969/j.issn.1005-0329.2019.10.001.

Teruo, Y. & Hiroshi, Y. 1977 *High-Velocity Jet Digging Method*. United State Patent No. 4047580.

Thomas, A. T. 1995 Surface roughening of metallic substrates by high pressure pure waterjet. *Surf. Coat. Technol.* **76-77**, 95–100. https://doi.org/10.1016/0257-8972(95)0252 8-6.

Wang, R. H. 2010 *Study on Rock Breaking Mechanism of High Pressure Water jet*. China University of Petroleum Press, Dongying, China.

Wang, W. D. & Zhou, Z. L. 1988 Pulsed gas-liquid jet rock-breaking device. *Wld. Min. Lett.* **36**, 21–22. https://doi.org/10.13828/j.cnki.ckjs.1988.36.015.

Xiang, W. Y., Lu, Y. Y., Li, X. H., Li, Q. & Feng, X. Y. 2006 Experimental study of the function of cavitating water jet on rock-cutting. *Rock Soil Mech.* **27** (9), 1505–1508. Available from: http://ytlx.whrsm.ac.cn/CN/Y2006/V27/I9/1505.

Xue, S. C., Zhang, Y., Ma, F., Gao, Y. & Xue, D. X. 2008 Application of high-pressure water jet in cleaning the inner surface of high pressure gas tube. *Oil Gas Storage Trans.* **27** (9), 45–47.

Zhao, J., Zhang, G. C., Xu, Y. J., Zhou, Y., Wang, R. Y., Xing, X. Y. & Li, J. B. 2017a SPH-based numerical simulation and experimental study on rock breaking by particle impact. *Explos. Shock Waves* **37** (3), 479–485. https://doi.org/10.11883/1001-1455(2017)03-0479-08.

Zhao, J., Zhang, G. C., Xu, Y. J., Wang, R. H., Zhou, W. D. & Yang, D. Y. 2017b Experimental and theoretical evaluation of solid particle erosion in an internal flow passage within a drilling bit. *J. Petrol. Sci. Eng.* **160**, 582–596. https://doi.org/10.1016/j.petrol.2017.10.068.

Zhao, J., Zhang, G. C., Xu, Y. J., Wang, R. H., Zhou, W. D. & Han, L. X. 2018 Bit internal flow passage erosion by solid-liquid two-phase flow impact of particles. *J. Cent. South Univ.* **49** (5), 1228–1236. https://doi.org/10.11817/j.issn.1672-7207.2018.05.026.

Zuo, J. H. & Liu, L. L. 2014 Study on derusting of freight car body by abrasive water jet. *Mech. MGT Dev.* **29** (4), 59–61. https://doi.org/10.16525/j.cnki.cn14-1134/th.2014.04.038.

First received 21 October 2022; accepted in revised form 21 January 2023. Available online 2 February 2023